REPORT

TBC1D8B Loss-of-Function Mutations Lead to X-Linked Nephrotic Syndrome via Defective Trafficking Pathways

Guillaume Dorval,[1,11] Valeryia Kuzmuk,[2,11] Olivier Gribouval,[1] Gavin I. Welsh,[2] Agnieszka Bierzynska,[2] Alain Schmitt,[3,4,5] Stéphanie Miserey-Lenkei,[6] Ania Koziell,[7] Shuman Haq,[8] Alexandre Benmerah,[1] Géraldine Mollet,[1] Olivia Boyer,[1,9] Moin A. Saleem,[2,11,*] and Corinne Antignac[1,10,11,*]

Steroid-resistant nephrotic syndrome (SRNS) is characterized by high-range proteinuria and most often focal and segmental glomerulosclerosis (FSGS). Identification of mutations in genes causing SRNS has improved our understanding of disease mechanisms and highlighted defects in the podocyte, a highly specialized glomerular epithelial cell, as major factors in disease pathogenesis. By exome sequencing, we identified missense mutations in *TBC1D8B* in two families with an X-linked early-onset SRNS with FSGS. TBC1D8B is an uncharacterized Rab-GTPase-activating protein likely involved in endocytic and recycling pathways. Immunofluorescence studies revealed TBC1D8B presence in human glomeruli, and affected individual podocytes displayed architectural changes associated with migration defects commonly found in FSGS. In zebrafish we demonstrated that both knockdown and knockout of the unique *TBC1D8B* ortholog-induced proteinuria and that this phenotype was rescued by human *TBC1D8B* mRNA injection, but not by either of the two mutated mRNAs. We also showed an interaction between TBC1D8B and Rab11b, a key protein in vesicular recycling in cells. Interestingly, both internalization and recycling processes were dramatically decreased in affected individuals' podocytes and fibroblasts, confirming the crucial role of TBC1D8B in the cellular recycling processes, probably as a Rab11b GTPase-activating protein. Altogether, these results confirmed that pathogenic variations in *TBC1D8B* are involved in X-linked podocytopathy and points to alterations in recycling processes as a mechanism of SRNS.

Steroid-resistant nephrotic syndrome (SRNS) is a glomerular disease characterized by massive proteinuria, most often associated with focal and segmental glomerulosclerosis (FSGS).[1] SRNS is responsible for chronic kidney disease and accounts for 15% of end-stage kidney disease (ESKD) cases in individuals under 25 years of age.[2] In glomeruli, podocytes are terminally differentiated, highly specialized epithelial cells. Podocyte foot processes (FPs) wrap the outer surface of the glomerular capillaries and interdigitate with FP of neighboring podocytes forming specialized cell-cell junctions called slit-diaphragms (SD), a major constituent of the glomerular filtration barrier. Identification of monogenic causes of SRNS involving more than 40 genes has helped decipher podocyte physiology.[3,4] Many studies have reported a strong relationship between the SD and the actin cytoskeleton,[4] and the role of vesicular trafficking has been well established in the maintenance of SD complexes.[5,6] Nevertheless, intracellular transport defects have rarely been related to monogenic SRNS.[7]

Now, through studies aiming at identifying new genes mutated in SRNS in two families, we identified a potential actor of endosomal trafficking. The first family (family A) was from Ecuador and presented with isolated congenital SRNS consistent with an X-linked inheritance. Pedigree and clinical features are described in Figure 1A and Table 1. Briefly, affected females (I-2 and II-2) exhibited non-nephrotic proteinuria, while affected boys (II-1, II-3, and II-4) developed congenital or early-onset NS. All pregnancies were marked by pre-eclampsia when carrying a male boy. In the proband (II-4) and her sister (II-2), kidney biopsy revealed FSGS lesions and electron microscopy (EM) showed FP effacement, a hallmark of NS.[1] The proband (II-4) reached ESKD by the age of 2.8 years and did not exhibit recurrence after kidney transplantation. By exome sequencing (ES), we identified a c.738G>C variant in *TBC1D8B* (GenBank: NM_198881.1; HGNC:24715) localized on chromosome X (Figure 1B). This missense variant (p.Gln246His) was defined as probably damaging by pathogenicity prediction software. Through a European collaborative network (Eurenomics), we identified another sporadic SRNS-affected individual (II-2) in a family (family B) originated from the UK Renal Rare Disease Registry (RaDaR #425), with a missense c.872T>C (p.Phe291Ser) variant in the same gene (Figures 1C and 1D, Table 1). This variant also displayed highly pathogenic scores. The affected individual (II-2), a male from European ancestry presenting with early-onset SRNS at the age of 2 years, had no other systemic features. Kidney biopsy

[1]Laboratory of Hereditary Kidney Diseases, Imagine Institute, INSERM U1163, Paris Descartes University, 75015 Paris, France; [2]Bristol Renal, University of Bristol and Bristol Royal Hospital for Children, Bristol, UK; [3]Inserm, U1016, Institut Cochin, 75014 Paris, France; [4]Cnrs, UMR8104, 75014 Paris, France; [5]Université Paris Descartes, Sorbonne Paris Cité, 75006 Paris, France; [6]Institut Curie, PSL Research University, CNRS, UMR 144, Molecular Mechanisms of Intracellular Transport, 75005 Paris, France; [7]Department of Children's Nephrology and Urology, Evelina London, London SE1 7EH, UK; [8]Paediatric Nephrology, University Hospital Southampton NHS Foundation Trust, Southampton SO16 6YD, UK; [9]Department of Pediatric Nephrology, Reference center for Hereditary Kidney Diseases (MARHEA), Necker Hospital, APHP, 75015 Paris, France; [10]Department of Genetics, Reference center for Hereditary Kidney Diseases (MARHEA), Necker Hospital, APHP,75015 Paris, France
[11]These authors contributed equally to this work
*Correspondence: m.saleem@bristol.ac.uk (M.A.S.), corinne.antignac@inserm.fr (C.A.)
https://doi.org/10.1016/j.ajhg.2018.12.016.

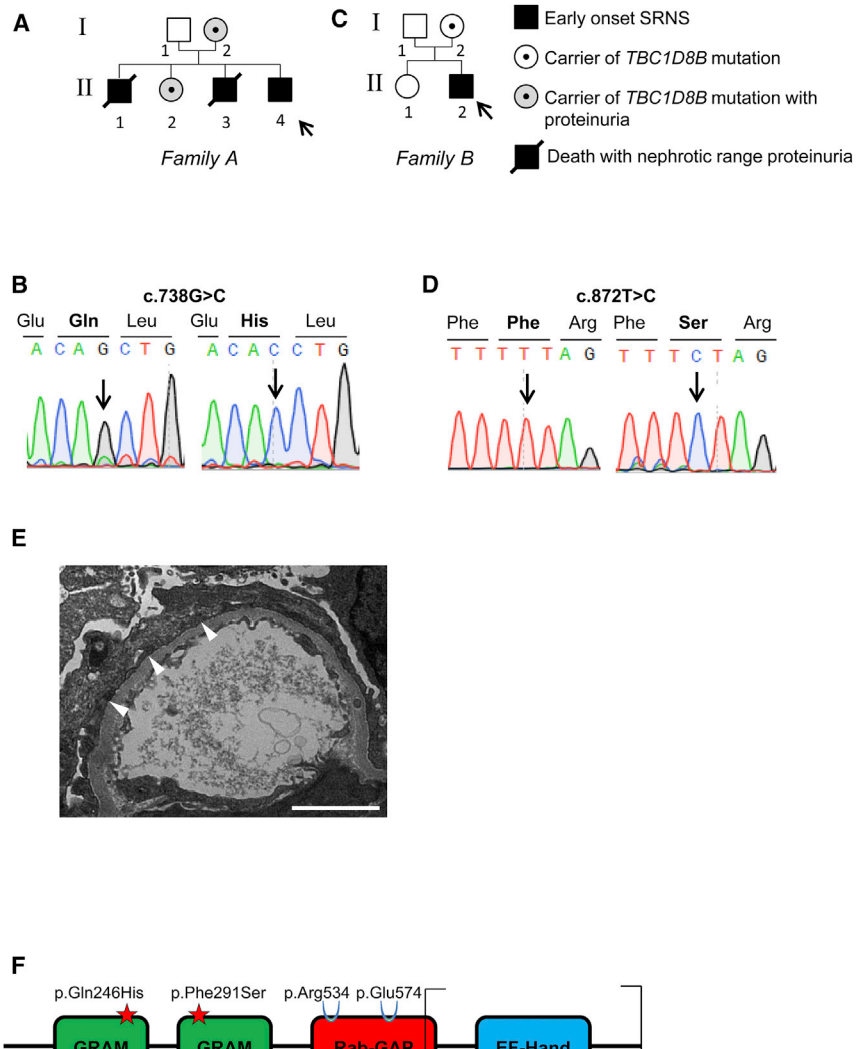

Figure 1. Clinical and Genetic Information for Families A and B

(A and C) Family pedigrees for families A (A) and B (C). In family A, the proband (II-4) and his brothers (II-1 and II-3) developed congenital nephrotic syndrome while the individual from family B (II-2) developed an early-onset nephrotic syndrome. Arrows indicate probands. *TBC1D8B* mutations c.738G>C and c.872T>C were detected in affected subjects and carriers of families A and B, respectively.

(B and D) Exome sequencing revealed two distinct missense variants in *TBC1D8B* (c.738G>C and c.872T>C). Segregation of variants was confirmed by Sanger sequencing in both families.

(E) Electron microscopy image from affected individual from family B (II-2) harboring the p.Phe291Ser mutation revealed foot processes effacement (white arrowheads) (scale bar, 2 μm).

(F) TBC1D8B protein exhibits two isoforms that include both mutations. Mutations localized in glucosyltransferases, Rab-like GTPase activators, and myotubularins (GRAM) domains at the N-terminal extremity. Catalytic residues on the Rab-GTPase activating (GAP) domain are maintained. C-terminal EF-hand domain is not conserved in isoform 2. EF-hand domain has been described in other proteins as a calcium-binding regulation site, which may downregulate the protein activity when bound to Ca^{2+}.[29]

revealed global sclerosis on light microscopy and FP effacement on EM (Figure 1E). He reached ESKD by the age of 9 years and underwent kidney transplantation a year later. Both mutations segregated with the affected status in the respective families and were, respectively, present in 1/27,314 (with no hemizygous) and absent from gnomAD database in the population-matched control subjects. Both mutations involved residues conserved from *C. elegans* to *H. sapiens* (Figures S1A and S1B). For the UK NephroS study, ethical approval was obtained from North Somerset & South Bristol Research Ethics Committee (reference 09/H0106/72 for data collection and reference 09/H0106/80 for sample collection and data analysis). French approval for human subjects research was obtained from the Comité de Protection des Personnes Ile de France II.

TBC1D8B is a member of the TBC domain protein family (Tre-2/Bub2/CDC16). Like other TBC proteins, TBC1D8B may function as a Rab-GTPase activating protein (Rab-GAP) by binding to specific Rab proteins and stimulating their GTPase activity.[8] Interestingly, in addition to its Rab-GAP (TBC) domain, TBC1D8B contains one GRAM domain repeated two times, which allows binding to lipid rafts, critical elements of SD signaling in podocytes.[9] The two mutations described above are localized within each GRAM domain (Figure 1F). TBC1D8B also possesses an EF-Hand domain localized at the C-terminal extremity. A second isoform of TBC1D8B results from alternative splicing events in intron 11 and leads to a shorter 632-amino acid protein, lacking the C-terminal extremity of the Rab-GAP domain and the entire EF-like domain. However, the catalytic residues (Arg534 and Glu574) are present in both protein isoforms.

The role of TBC1D8B has never been explored either in cell lines or animal models.

Immunofluorescence studies in human kidneys revealed the presence of TBC1D8B both in glomerular podocytes and tubules at early stages (25 weeks) and in mature kidney. In glomeruli, TBC1D8B colocalized with synaptopodin a specific cytosolic protein[10] (Figure 2A). To further comprehend the role of TBC1D8B, we undertook functional studies in both zebrafish and human podocytes. Podocytes from individual B (harboring the p.Phe291Ser

Table 1. Mutations in *TBC1D8B* in Two Families with a Likely X-Linked FSGS

Family	Individual	Ethnic Origin	Sex	Nucleotide Alteration	Exon	Satus	Protein Alteration	PolyPhen/Sift/MutationTaster	Amino Acid Conservation	Age at Proteinuria Onset	Immuno-sensitivity	Pathology	Age at ESRD	Age at Transplantation	Recurrence	Death
A	NCR2230 (index)	Ecuador	M	c.738G>C	5	hemi	p.Gln246His	0.996/0/DC	*C. elegans*	congenital	no	collapsing FSGS	2.8 years	4 years (thrombosis); 7 years	no	N/A
	NCR1387 (mother)	Ecuador	F			hetero				adult	N/A	N/A	no	N/A	N/A	N/A
	NCR1388 (sister)	Ecuador	F			hetero				7 years	no	FSGS	no	N/A	N/A	N/A
	brother 1	Ecuador	M	N/A	N/A	N/A	N/A	N/A	N/A	congenital	no	N/A	N/A	N/A	N/A	4 mo
	brother 2	Ecuador	M	N/A	N/A	N/A	N/A	N/A	N/A	5 months	no	N/A	N/A	N/A	N/A	14 mo
B	104	European	M	c.872T>C	6	hemi	p.Phe291Ser	0.961/0/DC	*C. elegans*	2 years	no	chronic progressive sclerosis	9 years	10 years	no	N/A

Abbreviations: M, male; F, female; mo, months; FSGS, focal and segmental glomerulosclerosis; hemi, hemizygous; hetero, heterozygous; N/A, not applicable; ESRD, end stage renal disease

variant) were conditionally immortalized from the affected individual's nephrectomy specimen using our published methodology.[11] As previously described in some monogenic SRNS, podocytes often display alterations in actin cytoskeleton organization[12–16] associated with changes in adhesion and migration.[14,17] Podocytes from affected individual B exhibited similar phenotypes, and TBC1D8B displayed an intracellular vesicular localization as shown in Figures 2B–2D. Podocytes from individual A were not available, since he underwent bilateral nephrectomy several years before.

According to the Zebrafish Genome Reference Consortium (GRCz11), *tbc1d8b* is the only zebrafish ortholog and is located on autosome 5. Only one transcript has been described corresponding to the longer isoform in humans. By whole-mount *in situ* hybridization in 24 post-fertilization (hpf) zebrafish embryos, we demonstrated *tbc1d8b* expression in the neural tube, brain, pectoral fins, and the pronephric glomerulus (Figure S2). Functional analyses were then performed in both *tbc1d8b* knock-down (KD) morphants and knock-out (KO) fish. Morphants were obtained by specifically targeting *tbc1d8b* with either splice-blocking (MO^{SPLICE}) or translation-blocking (MO^{ATG}) morpholino oligonucleotides. The efficacy of MO^{SPLICE} was checked by RT-PCR (Figure S3A), and the efficacy of MO^{ATG} was demonstrated by the absence of fluorescence after co-injection of the MO^{ATG} with its *tbc1d8b* 5′ UTR mRNA target fused to the GFP as described in Figure S3B. The *tbc1d8b*$^{-/-}$ mutant fish line was obtained by ENU mutagenesis resulting in a nonsense mutation in exon 9 (European Zebrafish Resource Center [EZRC]). The final product is a truncated 468-amino acid protein missing the Rab-GAP domain (which starts at residue 466). In zebrafish, pericardial edema has been previously reported to be an indirect marker of a glomerular filtration barrier defect and proteinuria,[16] although it is not specific and can be seen in other zebrafish abnormalities (i.e., heart defects, global developmental abnormalities). Such a phenotype was observed in >95% of both MO^{SPLICE} and MO^{ATG} morphants at 96 hpf whereas it was found in fewer than 2% of control MO fish at 96 hpf (Figures 3A and 3B). An identical phenotype was obtained in the *tbc1d8b*$^{-/-}$ fish with the expected Mendelian ratio (n = 261; 22.9% phenotype in *tbcd8b*$^{+/-}$ offspring; Figure 3C).

To characterize the effect of *tbc1d8b* loss on kidney anatomy, histology was performed and showed a retracted glomerulus in an enlarged Bowman's capsule in *tbc1d8b*$^{-/-}$ fish compared to controls (Figure 3D). Similar to affected individuals, EM revealed significant FP effacement and disappearance of SD in *tbc1d8b*$^{-/-}$ KO fish compared to controls (number of FP per μm 3.5 ± 0.2 and 5.3 ± 0.2, respectively - $p < 0.0001$) as indicated in Figures 3E and S4.

To confirm the glomerular permeability defect, we set up a dye-filtration assay. A high-molecular-weight FITC-labeled dextran (500 kDa) was injected in the cardinal vein of MO^{SPLICE} and $MO^{CONTROL}$ and *tbc1d8b*$^{-/-}$ or

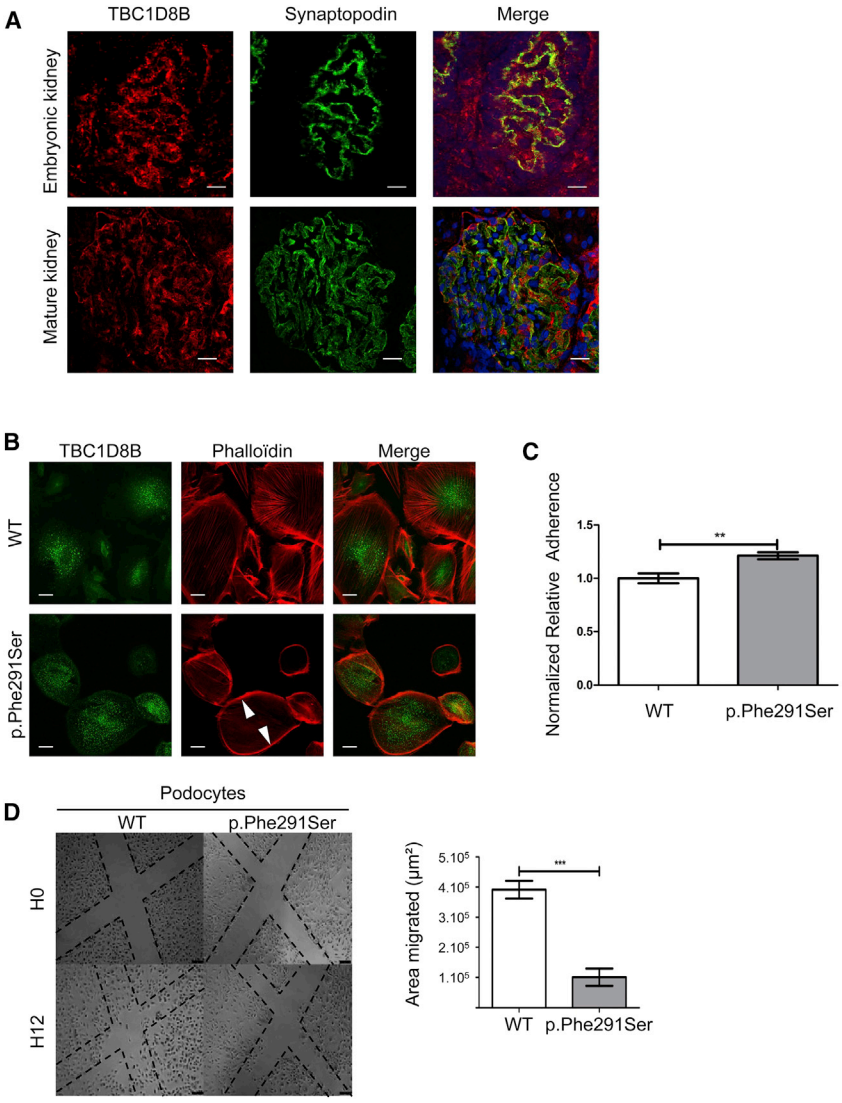

Figure 2. TBC1D8B Localization and Phenotype Observed in Mutated Podocytes

(A) Immunofluorescence studies were performed on human fetal kidney at 25 gestational weeks (top) and in mature kidney in a healthy 7-year-old male (bottom). TBC1D8B displayed a glomerular localization with partial colocalization with synaptopodin, a cytosolic podocyte protein (scale bar, 20 μm).

(B) In immunofluorescence experiments in immortalized podocytes, TBC1D8B displayed an intracellular vesicular expression. F-actin cytoskeleton was detected by immunofluorescence with phalloidin staining. p.Phe291Ser human mutant podocytes cortically (arrowhead) reorganized their F-actin cytoskeleton. Original magnification ×63.

(C) Cell adhesion was measured with a spectrophotometer at 570 nm optical density ($n = 3$, $^{**}p < 0.01$, mean ± SEM).

(D) Human podocyte cell motility and migration were measured by scratch assays. Number of cells per unit was significantly higher in the WT group 12 hr after the scratch as shown on the graph on right ($n = 3$, $^{***}p < 0.0001$, mean ± SEM).

tbc1d8b^{WT} zebrafish at 96 hpf. We then screened the filtration defects in two different ways. We first measured fluorescence in the retinal vein and showed that fluorescence in the vasculature of MO^{SPLICE} fish was significantly decreased compared to MO^{CONTROL} (Figure S5). We then showed specific glomerular leakage by imaging dye uptake in tubular cells 6 h post-injection (6 hpi). Fluorescence was observed in tubular cells in KO *tbc1d8b*$^{-/-}$ fish, but not in control fish, revealing a glomerular protein leakage consistent with pericardial edema and EM findings (Figure 3F).

To investigate the functional consequences of both mutations, we performed rescue experiments in zebrafish using the human short isoform of WT and mutant mRNAs, since in wild-type human cultured podocytes, the 632-amino acid short isoform seems to be predominantly expressed (Figure S6). As mentioned previously, edema was described in 97.6% of morphants. However, when mRNA^{WT} (100 pg) was co-injected with MO, this ratio fell to 16% ($n = 148$) (Figure 3G) with a dose-response effect (Figure S7). Conversely, the mutated mRNA$^{p.Gln246His}$ and mRNA$^{p.Phe291Ser}$ were only able to very partially rescue the phenotype with 80% ($n = 201$) and 68% ($n = 282$) of fish exhibiting pericardial edema, respectively (Figure 3G). These results indicate that although both mutations are clearly damaging in both individuals, a modest protein residual activity is likely.

As mentioned above, TBC1D8B may act as Rab-GAP, promoting GTP hydrolysis in specific Rab proteins.[18] In mammalian cells including podocytes, Rab-GTPases are mostly involved in vesicular trafficking.[19,20] To further analyze the role of TBC1D8B in this process, we performed transferrin endocytosis and recycling assays in affected individuals' podocytes and fibroblasts harboring p.Phe291Ser and p.Gln246His variants, respectively. Transferrin is a widely used marker for both clathrin-mediated internalization and recycling pathways in most cell types. After internalization from the plasma membrane and before being recycled back to cell surface, transferrin and its receptor accumulate in the perinuclear recycling compartment (PNRC).[21,22] We detected a delay in transferrin uptake in affected individuals' cells compared to control subjects. After 15 and 60 min of incubation (in fibroblasts and podocytes, respectively), most of the fluorescence was found in the PNRC of WT cells. However, endocytosis was significantly slower in mutant fibroblasts and podocytes (Figures 4A, 4B, S8A, and S8B). In addition, analysis of transferrin recycling revealed a significant decrease of normalized fluorescence intensity 45 min after transferrin loading in WT podocytes as well as in fibroblasts, whereas it was maintained in the PNRC

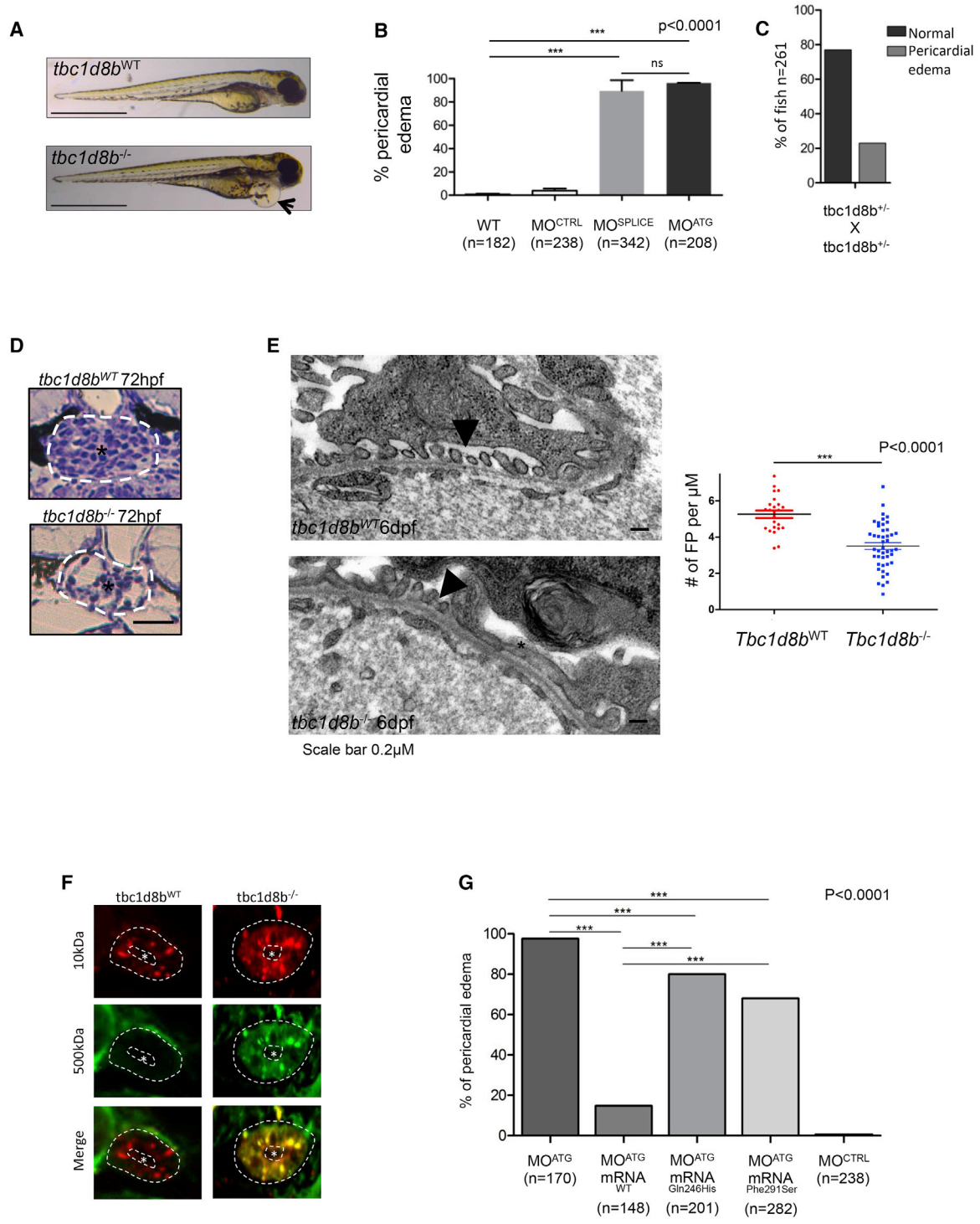

Figure 3. Phenotype Observed in *tbc1d8b* KO and KD Zebrafish

(A) KO fish displayed pericardial edema at 48 hpf on mutant fish (black arrow). Scale bar, 1 mm.

(B) Both MO^{ATG} and MO^{SPLICE} also exhibited pericardial edema in more than 95% fish whereas $MO^{CONTROL}$ did not ($n > 200$, ***$p < 0.0001$, mean ± SEM).

(C) *tbc1d8b*$^{+/-}$ offspring displayed pericardial edema with a Mendelian ratio.

(D) Regular optical microscopy revealed a retracted glomerulus (*) in an enlarged Bowman's capsule (white circle) in mutated *tbc1d8b*$^{-/-}$ fish compared to control (scale bar, 15 µm).

(E) Electron microscopy findings showed a mixture of foot processes (FP) effacement (*) with regular FP (black arrowheads). Graph on the right shows a significantly lower rate of FP per uM in *tbc1d8b*$^{-/-}$ fish compared to control ($n = 3$ fish per condition, ***$p < 0.001$, mean ± SEM).

(legend continued on next page)

in affected individuals' cells (Figures 4C, 4D, S8C, and S8D). Altogether, these results strongly suggest that both endocytosis and vesicular recycling are altered in affected podocytes.

In cells, PNRC dynamics and recycling are mostly regulated by Rab11. We then hypothesized that TBC1D8B might be a crucial GAP for Rab11 that displays at least two isoforms (Rab11a and Rab11b)[22] both present in mouse podocytes.[23] By co-immunoprecipitation experiments in HEK293T cells, we showed that the Rab-binding domain (RBD) of TBC1D8B was able to interact with a dominant active, GTP-bound, mutant of Rab11b (DA-Rab11b), but not with DA-Rab11a (Figures 4E and 4F). We also observed a specific interaction between endogenous TBC1D8B and DA-Rab11b (Figure 4G). In addition, we showed that DA-Rab11b and TBC1D8B Rab-binding domain colocalized at the PNRC when co-expressed in podocytes (Figure S9), but interestingly, the widespread Rab11b signal in WT cells shifted to a very restricted localization to the PNRC in mutant podocytes, which suggests that GTP-bound Rab11b is trapped in the PNRC in cells from affected individuals (Figures S10A and S10B). Altogether, these data strongly suggest that TBC1D8B is a specific Rab11b-GTPase activating protein.

Numerous proteins are subject to Rab11-dependent recycling in various cell types, especially in neurons.[24] However, although it has been shown that some proteins are recycled in a Rab11b-dependent manner,[25] only a few studies explored the role of Rab11b on vesicular trafficking. In 2016, Grimsey et al. reported the crucial role of Rab11b GTP hydrolysis for the initiation of transferrin recycling from the PNRC to the plasma membrane.[26] In podocytes SD integrity is of utmost importance and several SD proteins are subjected to endocytic and recycling events to maintain their regulation.[27] Very recently, mutations in *GAPVD1*, a Rab5 effector showed to be involved in nephrin regulation at the SD, were reported as disease causing.[7] In our study, we did not find any interaction between TBC1D8B and Rab5 (Figure 4F), suggesting that Rab5 is not a target of TBC1D8B. Thus, our results highly suggest that some podocyte-specific proteins could specifically use the Rab11b-dependent recycling pathway, as it has been shown for some SD proteins and the use of the Rab5-dependent pathway.[7] By this means, alterations in Rab11b activation would lead to SD dysregulation, implying that not only endocytosis but also recycling are of fundamental importance for SD integrity. Indeed, it is likely that mutations in *TBC1D8B* lead to strong defect in recycling processes in podocytes, which could also induce a defect in transferrin uptake linked to decrease number of receptors at the plasma membrane at steady state.

Altogether, our results confirmed that mutations in *TBC1D8B* are involved in the development of early SRNS in rare affected individuals. We show herein that vesicular trafficking plays a fundamental role in podocyte disease, especially in SRNS, through a Rab11-dependent recycling process. Recent discoveries in monogenic SRNS and especially in SD regulation during disease through endocytic and recycling pathways would certainly help to develop targeted therapy for affected individuals.

Supplemental Data

Supplemental Data include 11 figures, 1 table, and Supplemental Material and Methods and can be found with this article online at https://doi.org/10.1016/j.ajhg.2018.12.016.

Acknowledgments

We express gratitude to the affected individuals and their families for contributing to improve medical knowledge in nephrotic syndrome. We thank Imagine's platform of cell imaging for help in images acquisition, and the Bioinformatics Platform of Paris Descartes University and the Imagine Genomics Platform for exome sequencing. We also thank the MRC in addition to the Wolfson Foundation for establishing the Wolfson Bioimaging Facility, University of Bristol. We thank Prof. Iain Drummond, Dr. Marion Delous, and Dr. MC. Gubler for helpful discussion and Elizabeth Angus (Southampton) for EM images.

This research was supported by the Investments for the Future Program (grant ANR-10-IAHY-01 to C.A.), the European Union's Seventh Framework Programme (FP7/2007–2013) grant 305608 (EURenOmics) (to C.A.), and the Fondation Recherche Medicale (project DEQ2015031682) (to C.A.). This research was also supported by grants from Kidney Research UK, NIHR-TRC, Nephrotic Syndrome Trust, and the National Institute for Health Research (NIHR) Biomedical Research Centre based at Guy's and St Thomas' NHS Foundation Trust and King's College London. G.D. was supported by the "Programme Santé-Science" (MD-PhD) of Imagine Institute and Fondation Bettencourt Schueller, France. V.K. was supported by a Kidney Research UK PhD studentship.

The UK affected individuals were recruited via NephroS, the National Nephrotic Syndrome Study based within RaDaR, the UK renal Rare Disease Registry.

Declaration of Interests

The authors declare no competing interests.

Received: September 10, 2018
Accepted: December 20, 2018
Published: January 17, 2019

(F) Dye filtration assay was performed in KO and control fish. While Texas-Red 10 kDa fluorescence uptake was physiologically found in both *tbc1d8b*$^{-/-}$ and $^{+/-}$, FITC 500 kDa fluorescence was only found in KO fish (n = 3). Asterisk represents tubular lumen (scale bar, 5 μm).
(G) In rescue experiments, only human WT mRNA was able to significantly decrease pericardial edema whereas both mutated mRNA were able to only partially reduce phenotype in fish (n > 100/condition).

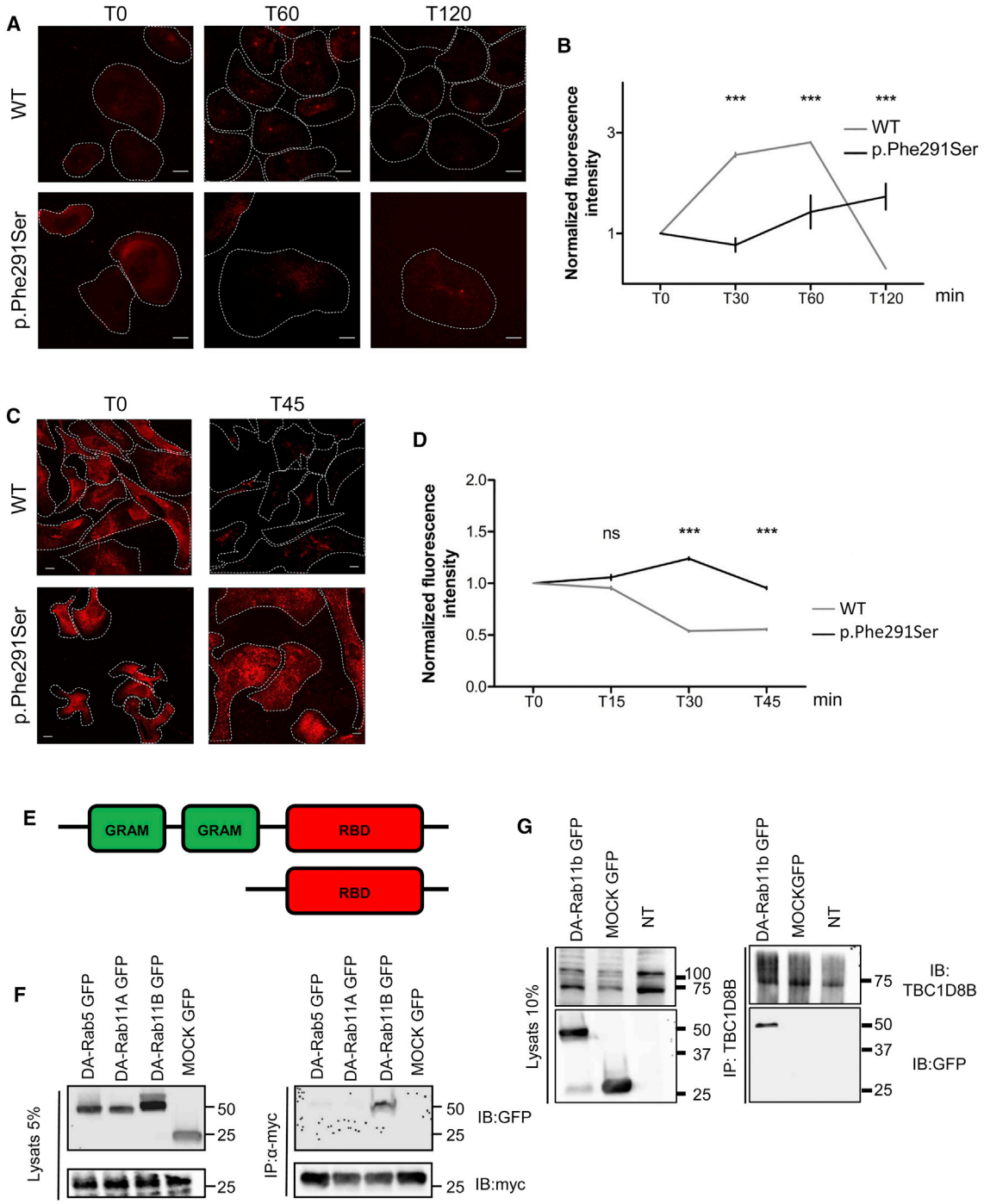

Figure 4. TBC1D8B Interaction and Effect of Mutations on Vesicular Trafficking

(A and B) Transferrin uptake is evaluated by incubation with fluorescently labeled transferrin. Fluorescence intensity progressively increased in control podocytes whereas it increased much more slowly in mutated podocytes harboring the p.Phe291Ser mutation suggesting an endocytosis defect. Graph B represents the quantification of normalized fluorescence in both mutated and control cells (***$p < 0.001$, mean ± SEM; scale bar, 25 μm).

(C and D) Transferrin chase evaluates the recycling process in podocytes. Measuring recycling of fluorescently labeled transferrin in WT and mutant podocytes revealed persistence of fluorescence 45 min after internalization in mutant cells while it reached 50% of T0 intensity in control podocytes, indicating a delay in recycling processes in mutant cells (C). Graph D represents the quantification of normalized fluorescence in both mutated and control cells (***$p < 0.001$ at 45 min, mean ± SEM; scale bar, 25 μm).

(E) Construct used for to perform co-immunoprecipitation with a specific plasmid harboring only the TBC1D8B Rab-binding domain (RBD) tagged with the myc epitope, and under the CMV promoter.

(F) In co-transfected HEK293T, we showed that the (myc-)RBD of TBC1D8B was able to interact with Dominant Active (DA)-Rab11b but not DA-Rab11A nor DA-Rab5.

(G) The endogenous TBC1D8B protein interacts with transfected DA-Rab11b-GFP in HEK cells.

Web Resources

Eurenomics, https://eurenomics.eu/
GenBank, https://www.ncbi.nlm.nih.gov/genbank/
gnomAD, http://gnomad.broadinstitute.org/
MutationTaster, http://www.mutationtaster.org/
OMIM, http://www.omim.org/
PolyPhen, http://genetics.bwh.harvard.edu
Praline, http://www.ibi.vu.nl/programs/pralinewww/
SIFT, http://sift.jcvi.org

References

1. D'Agati, V. (2003). Pathologic classification of focal segmental glomerulosclerosis. Semin. Nephrol. *23*, 117–134.
2. Smith, J.M., Stablein, D.M., Munoz, R., Hebert, D., and McDonald, R.A. (2007). Contributions of the Transplant Registry: The 2006 Annual Report of the North American Pediatric Renal Trials and Collaborative Studies (NAPRTCS). Pediatr. Transplant. *11*, 366–373.
3. Lovric, S., Ashraf, S., Tan, W., and Hildebrandt, F. (2016). Genetic testing in steroid-resistant nephrotic syndrome: when and how? Nephrol. Dial. Transplant. *31*, 1802–1813.
4. Bierzynska, A., McCarthy, H.J., Soderquest, K., Sen, E.S., Colby, E., Ding, W.Y., Nabhan, M.M., Kerecuk, L., Hegde, S., Hughes, D., et al. (2017). Genomic and clinical profiling of a national nephrotic syndrome cohort advocates a precision medicine approach to disease management. Kidney Int. *91*, 937–947.
5. Faul, C., Asanuma, K., Yanagida-Asanuma, E., Kim, K., and Mundel, P. (2007). Actin up: regulation of podocyte structure and function by components of the actin cytoskeleton. Trends Cell Biol. *17*, 428–437.
6. Tossidou, I., Teng, B., Menne, J., Shushakova, N., Park, J.K., Becker, J.U., Modde, F., Leitges, M., Haller, H., and Schiffer, M. (2010). Podocytic PKC-alpha is regulated in murine and human diabetes and mediates nephrin endocytosis. PLoS ONE *5*, e10185.
7. Hermle, T., Schneider, R., Schapiro, D., Braun, D.A., van der Ven, A.T., Warejko, J.K., Daga, A., Widmeier, E., Nakayama, M., Jobst-Schwan, T., et al. (2018). *GAPVD1* and *ANKFY1* Mutations Implicate RAB5 Regulation in Nephrotic Syndrome. J. Am. Soc. Nephrol. *29*, 2123–2138.
8. Fukuda, M. (2011). TBC proteins: GAPs for mammalian small GTPase Rab? Biosci. Rep. *31*, 159–168.
9. Huber, T.B., Schermer, B., Müller, R.U., Höhne, M., Bartram, M., Calixto, A., Hagmann, H., Reinhardt, C., Koos, F., Kunzelmann, K., et al. (2006). Podocin and MEC-2 bind cholesterol to regulate the activity of associated ion channels. Proc. Natl. Acad. Sci. USA *103*, 17079–17086.
10. Welsch, T., Endlich, N., Gökce, G., Doroshenko, E., Simpson, J.C., Kriz, W., Shaw, A.S., and Endlich, K. (2005). Association of CD2AP with dynamic actin on vesicles in podocytes. Am. J. Physiol. Renal Physiol. *289*, F1134–F1143.
11. Saleem, M.A., O'Hare, M.J., Reiser, J., Coward, R.J., Inward, C.D., Farren, T., Xing, C.Y., Ni, L., Mathieson, P.W., and Mundel, P. (2002). A conditionally immortalized human podocyte cell line demonstrating nephrin and podocin expression. J. Am. Soc. Nephrol. *13*, 630–638.
12. Asanuma, K., Kim, K., Oh, J., Giardino, L., Chabanis, S., Faul, C., Reiser, J., and Mundel, P. (2005). Synaptopodin regulates the actin-bundling activity of alpha-actinin in an isoform-specific manner. J. Clin. Invest. *115*, 1188–1198.
13. Akilesh, S., Suleiman, H., Yu, H., Stander, M.C., Lavin, P., Gbadegesin, R., Antignac, C., Pollak, M., Kopp, J.B., Winn, M.P., and Shaw, A.S. (2011). Arhgap24 inactivates Rac1 in mouse podocytes, and a mutant form is associated with familial focal segmental glomerulosclerosis. J. Clin. Invest. *121*, 4127–4137.
14. Ashraf, S., Gee, H.Y., Woerner, S., Xie, L.X., Vega-Warner, V., Lovric, S., Fang, H., Song, X., Cattran, D.C., Avila-Casado, C., et al. (2013). ADCK4 mutations promote steroid-resistant nephrotic syndrome through CoQ10 biosynthesis disruption. J. Clin. Invest. *123*, 5179–5189.
15. Gee, H.Y., Saisawat, P., Ashraf, S., Hurd, T.W., Vega-Warner, V., Fang, H., Beck, B.B., Gribouval, O., Zhou, W., Diaz, K.A., et al. (2013). ARHGDIA mutations cause nephrotic syndrome via defective RHO GTPase signaling. J. Clin. Invest. *123*, 3243–3253.
16. Gee, H.Y., Zhang, F., Ashraf, S., Kohl, S., Sadowski, C.E., Vega-Warner, V., Zhou, W., Lovric, S., Fang, H., Nettleton, M., et al. (2015). KANK deficiency leads to podocyte dysfunction and nephrotic syndrome. J. Clin. Invest. *125*, 2375–2384.
17. Tamura, H., Nakazato, H., Kuraoka, S., Yoneda, K., Takahashi, W., and Endo, F. (2016). Reduced INF2 expression in nephrotic syndrome is possibly related to clinical severity of steroid resistance in children. Nephrology (Carlton) *21*, 467–475.
18. Kramer-Zucker, A.G., Wiessner, S., Jensen, A.M., and Drummond, I.A. (2005). Organization of the pronephric filtration apparatus in zebrafish requires Nephrin, Podocin and the FERM domain protein Mosaic eyes. Dev. Biol. *285*, 316–329.
19. Pan, X., Eathiraj, S., Munson, M., and Lambright, D.G. (2006). TBC-domain GAPs for Rab GTPases accelerate GTP hydrolysis by a dual-finger mechanism. Nature *442*, 303–306.
20. Pfeffer, S.R. (2017). Rab GTPases: master regulators that establish the secretory and endocytic pathways. Mol. Biol. Cell *28*, 712–715.
21. Grant, B.D., and Donaldson, J.G. (2009). Pathways and mechanisms of endocytic recycling. Nat. Rev. Mol. Cell Biol. *10*, 597–608.
22. Mukherjee, S., Ghosh, R.N., and Maxfield, F.R. (1997). Endocytosis. Physiol. Rev. *77*, 759–803.
23. Kann, M., Ettou, S., Jung, Y.L., Lenz, M.O., Taglienti, M.E., Park, P.J., Schermer, B., Benzing, T., and Kreidberg, J.A. (2015). Genome-Wide Analysis of Wilms' Tumor 1-Controlled Gene Expression in Podocytes Reveals Key Regulatory Mechanisms. J. Am. Soc. Nephrol. *26*, 2097–2104.
24. Lapierre, L.A., Dorn, M.C., Zimmerman, C.F., Navarre, J., Burnette, J.O., and Goldenring, J.R. (2003). Rab11b resides in a vesicular compartment distinct from Rab11a in parietal cells and other epithelial cells. Exp. Cell Res. *290*, 322–331.
25. Li, X., and DiFiglia, M. (2012). The recycling endosome and its role in neurological disorders. Prog. Neurobiol. *97*, 127–141.
26. Grimsey, N.J., Coronel, L.J., Cordova, I.C., and Trejo, J. (2016). Recycling and Endosomal Sorting of Protease-activated Receptor-1 Is Distinctly Regulated by Rab11A and Rab11B Proteins. J. Biol. Chem. *291*, 2223–2236.
27. Inoue, K., and Ishibe, S. (2015). Podocyte endocytosis in the regulation of the glomerular filtration barrier. Am. J. Physiol. Renal Physiol. *309*, F398–F405.
29. Gallo, L.I., Liao, Y., Ruiz, W.G., Clayton, D.R., Li, M., Liu, Y.J., Jiang, Y., Fukuda, M., Apodaca, G., and Yin, X.M. (2014). TBC1D9B functions as a GTPase-activating protein for Rab11a in polarized MDCK cells. Mol. Biol. Cell *25*, 3779–3797.

The American Journal of Human Genetics, Volume *104*

Supplemental Data

TBC1D8B Loss-of-Function Mutations Lead to X-Linked Nephrotic Syndrome via Defective Trafficking Pathways

Guillaume Dorval, Valeryia Kuzmuk, Olivier Gribouval, Gavin I. Welsh, Agnieszka Bierzynska, Alain Schmitt, Stéphanie Miserey-Lenkei, Ania Koziell, Shuman Haq, Alexandre Benmerah, Géraldine Mollet, Olivia Boyer, Moin A. Saleem, and Corinne Antignac

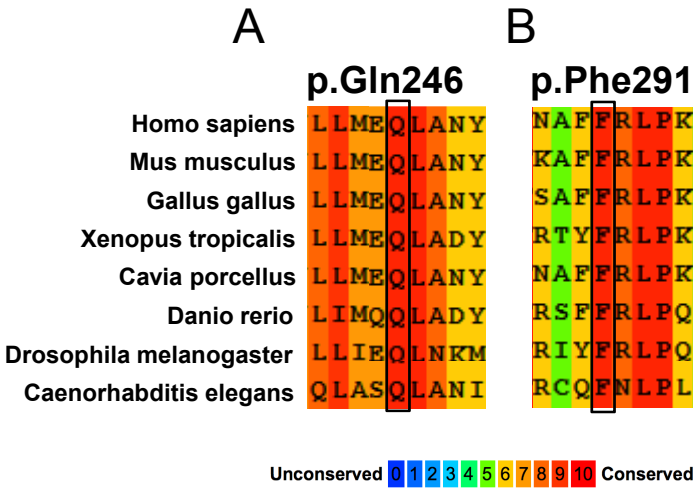

Figure S1- TBC1D8B amino-acids conservation
Amino-acids alignments of p.Gln246 and p.Phe291 revealed conservation of both amino-acids from *C. elegans*.

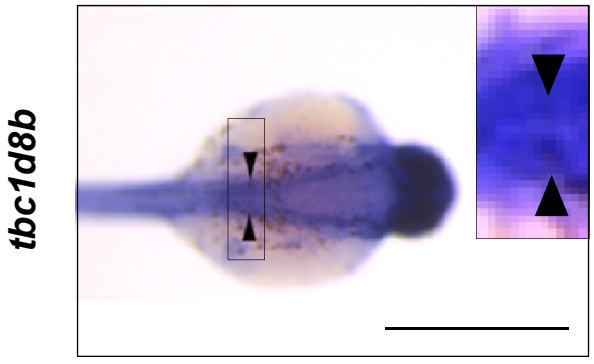

Figure S2 – tbc1d8b in situ hybridization in zebrafish larvae
In situ hybridization experiments revealed expression in the brain, neural tubes, pectoral fins and the pronephric glomeruli at 24hpf. Square shows pronephric glomeruli at higher magnification. Black arrowheads indicate unfused glomeruli on each side of median line. Scale bar 500µm.

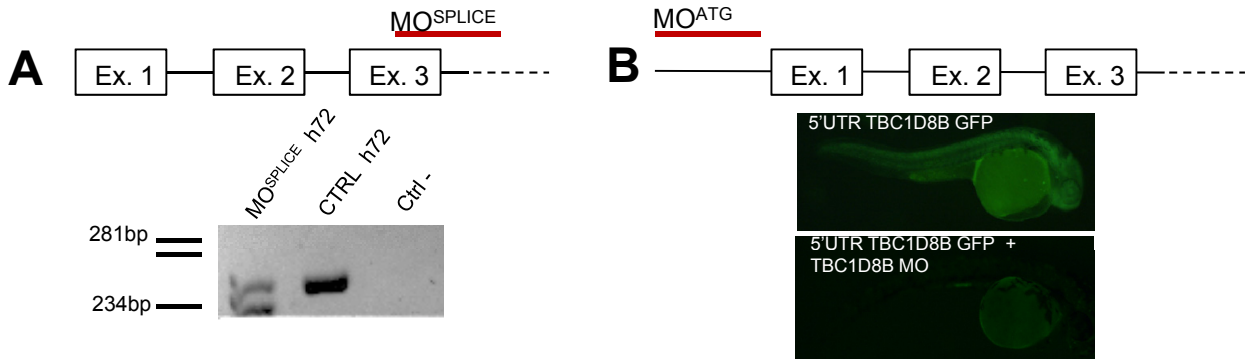

Figure S3 - Verification of both initiation blocking and splice MO specificity

(A) PCR from MO^{SPLICE} cDNA specimen showed an extra-band at 224bp compared to WT cDNA.

(B) Embryos injected with MO^{ATG} and its corresponding sequence mRNA fused to GFP showed a significant decreased in fluorescence compared to embryos injected with mRNA only.

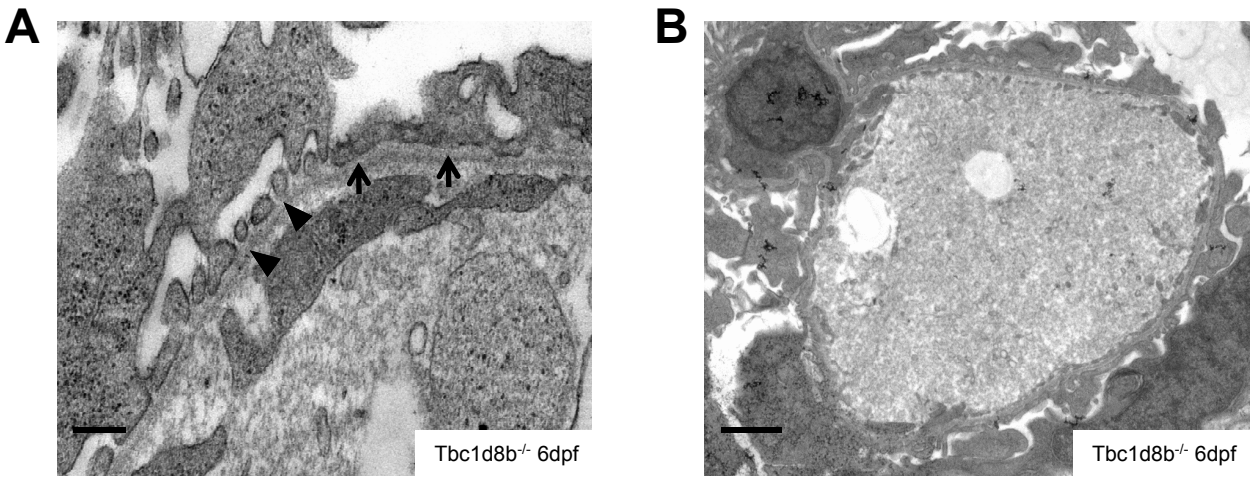

Figure S4 - Electron microscopy of zebrafish glomeruli

Electron microscopy revealed at high magnification (A-5000X) an alternance of regular foot processes (arrowheads) and foot process effacement (arrows). This architecture is found all around glomerular basement membrane at lower magnification (B- 1500X). Scale bar = 0.2µm

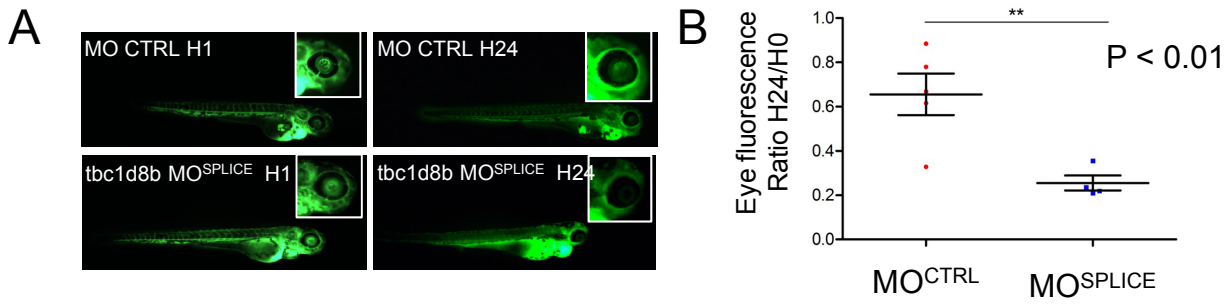

Figure S5 – Dye filtration eye assay in zebrafish
Measurements of fluorescence in retinal vein of WT and morphants zebrafish revealed a significant decreased in morphants, suggesting a pathological protein loss by fish (**,p<0.01).

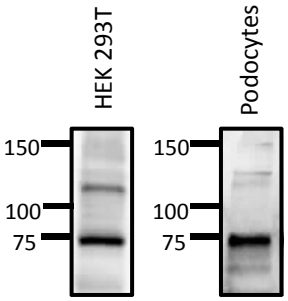

Figure S6 -TBC1D8B expression in cultured podocytes and KEK293T cells
Western-blot of TBC1D8B revealed expression of a band around 75kDa in cultured differentiated podocytes, demonstrating the expression of the isoform 2 expected to migrate at 73kDa. In HEK293T cells, both isoforms were present even if the shorter one seems to be predominant (not quantified).

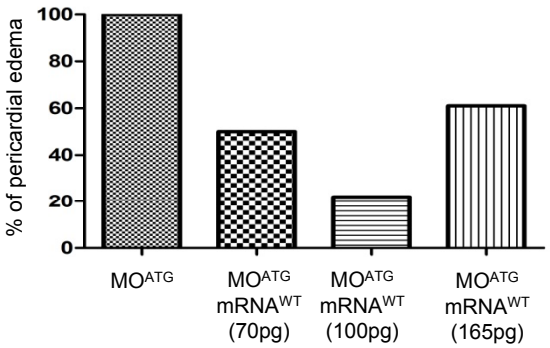

Figure S7 – Dose-response effect of TBC1D8B human mRNA injection in morphants zebrafish
Injection of TBC1D8B WT mRNA in zebrafish morphants induced a dose-dependent response. Dose > 100pg induced embryo toxicity with aberrant phenotype such as cyclops.

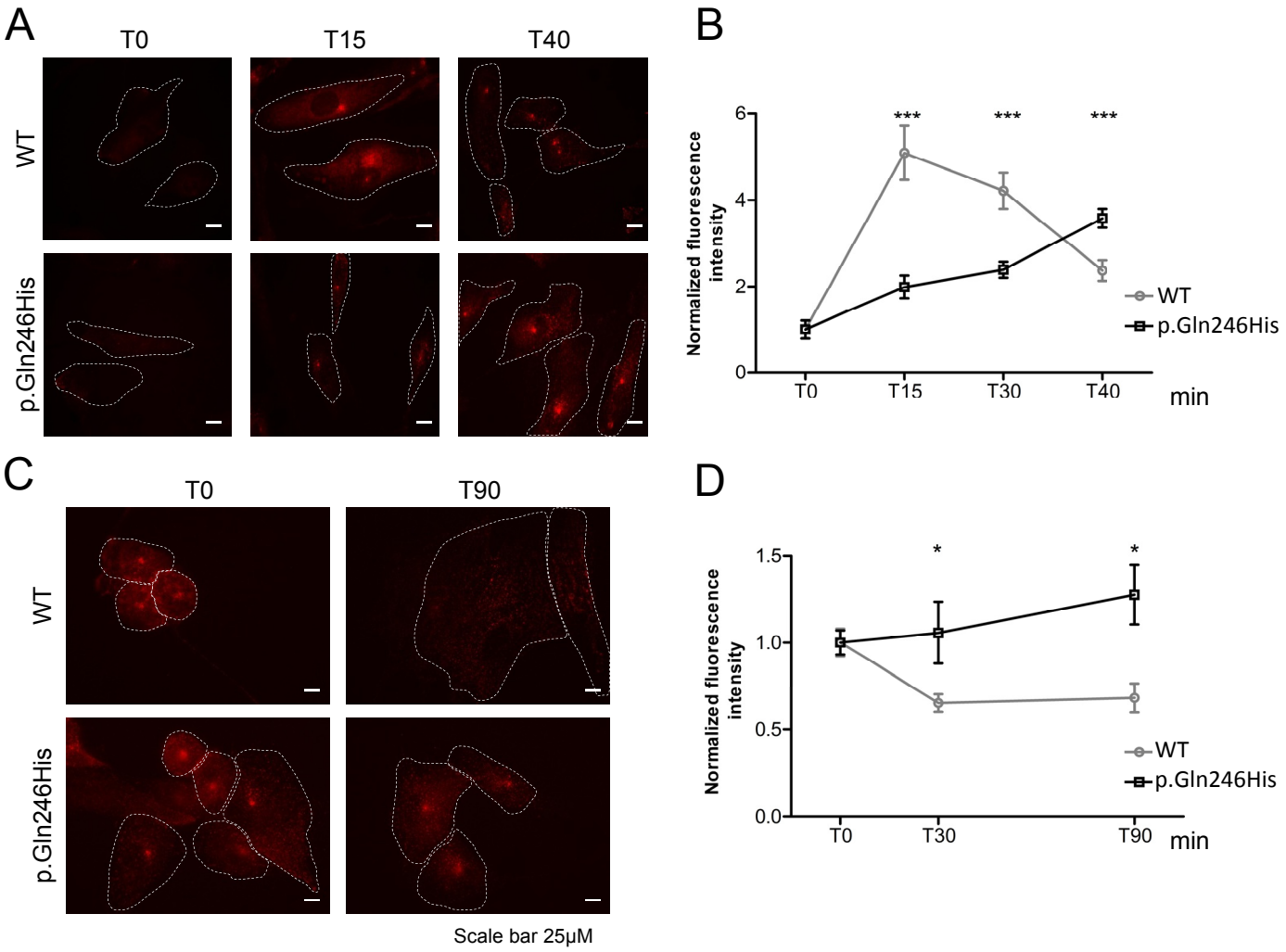

Figure S8- Transferrin assay in mutated fibroblasts harboring the p.Gln246His mutation and control

A-B After incubation with fluorescent labeled transferrin, intensity rapidly increased in control fibroblasts whereas fluorescence increasing was significantly slower in mutated cells harboring the p.Gln246His mutation. Graph B represents the quantification of normalized fluorescence in both mutated and control cells (***,$p<0.001$, mean±SEM). (Scale bar 25µm)

C-D Measuring of labeled-transferrin recycling in WT and mutated fibroblasts revealed a maintenance of fluorescence 90min after internalization in mutant cells while it was almost negative in control podocytes (***,$p<0.01$ at 90min, mean±SEM). (Scale bar 25µm)

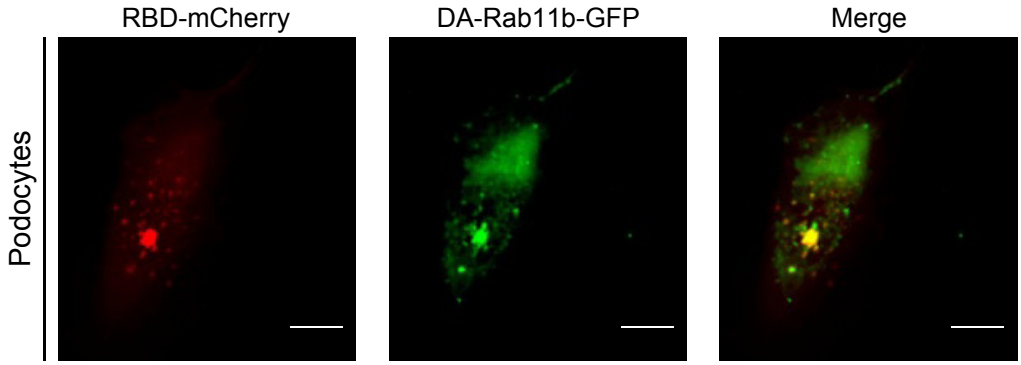

Figure S9- Cellular localization of DA-Rab11b and the Rab-Binding-Domain (RBD) of TBC1D8B in podocytes
In co-transfected podocytes, RBD-mCherry showed a partial colocalization with DA-Rab11b-GFP at the perinuclear recycling compartment. Scale bar 10µM

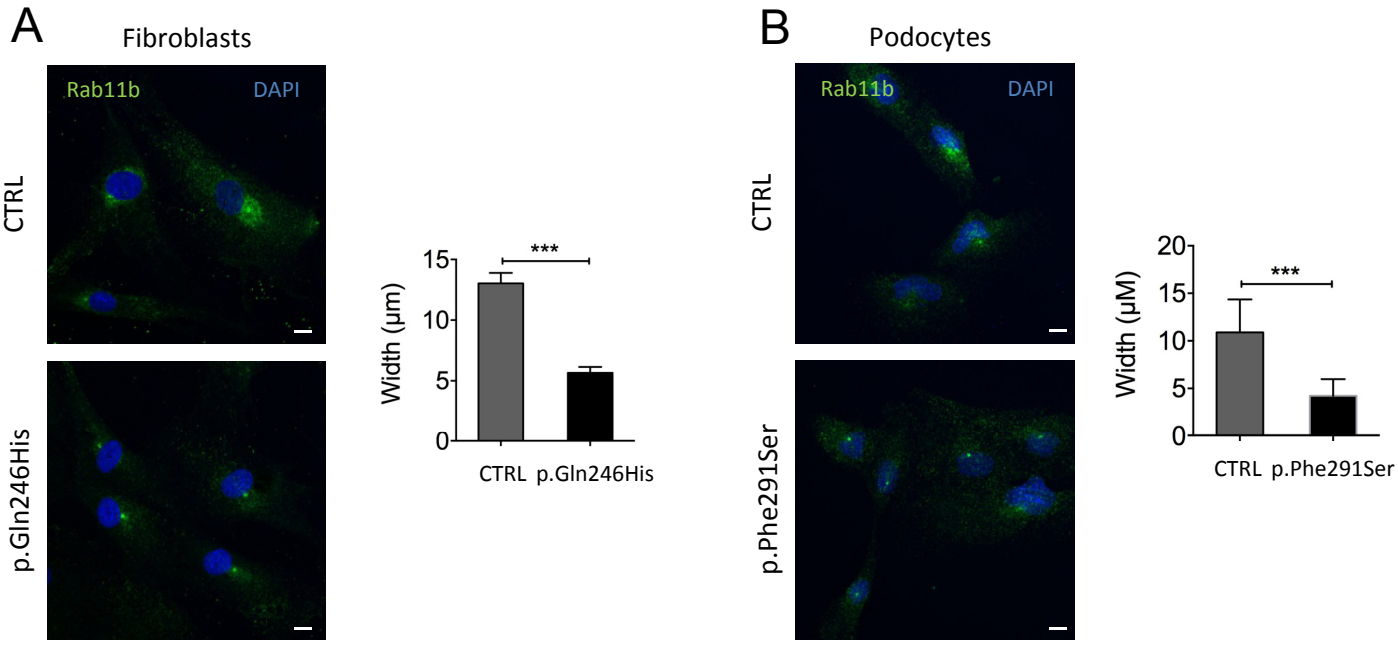

Figure S10- Cellular localization of endogenous Rab11b
In mutant fibroblasts and podocytes, Rab11b exhibits a restricted localization to the perinuclear compartment compared to WT cells. Scale bar 10µM

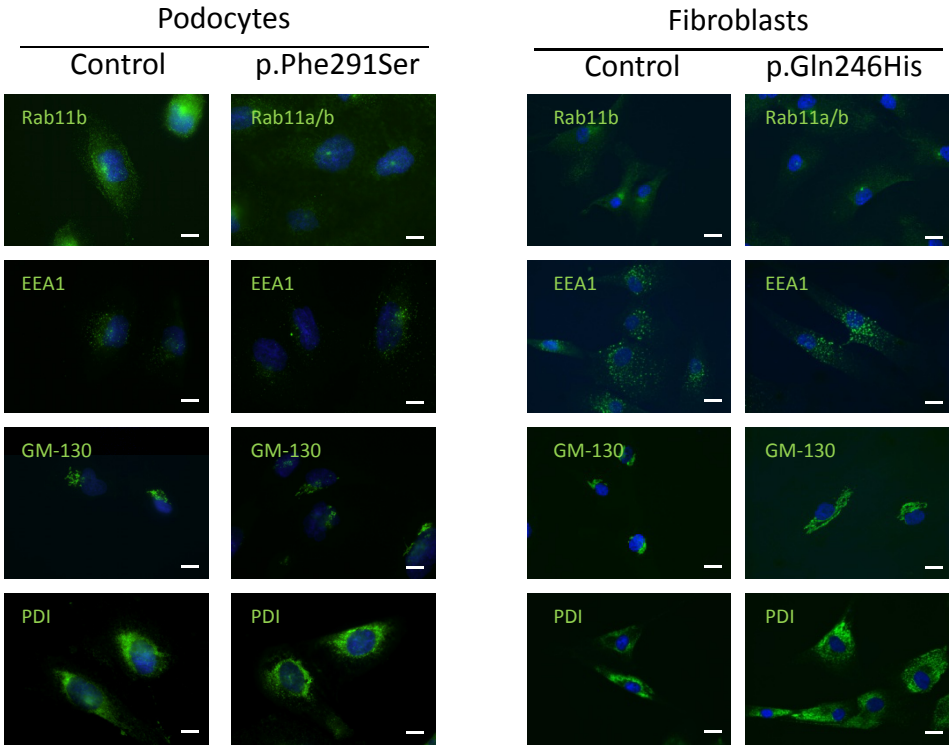

Figure S11 – Immunofluorescence staining of cellular compartment in affected individuals and controls

In affected individuals and control fibroblasts and podocytes, only Rab11b (on the top line) exhibited a particular phenotype described in the figure S10. Staining of early endosomes (EEA1), golgi (GM-130) or endoplasmic reticulum (PDI) are the same in affected individuals and controls.

Primers	**Sequence**
TBC1D8B Rab Binding Domain F for pCS2-GFP	TAGGGATCCGCCACCATGGGACGTGGTGTTAGTATGTTTCG
TBC1D8B Rab Binding Domain R for pCS2-GFP	TAGGAATTC**CG**GTCAAAGAACCTGTTTAAGGCTGTC
TBC1D8B Rab Binding Domain F for pmCherry-NI	TAGGGTACCGCCACCATGGGACGTGGTGTTAGTATGTTTCG
TBC1D8B Rab Binding Domain R for pmCherry-NI	ATGGGATCCAGGTCAAAGAACCTGTTTAAGGCTGTC
Rab11b F for pCS2-GFP	TAGGGATCCGCCACCATGATGGGGACCCGGGACGACG
Rab11b R for pCS2-GFP	TAGGAATTC**CG**CAGGTTCTGGCAGCACTGCA
MO^{SPLICE} F	GCTTGCTGGTCGGAACCTTGG
MO^{SPLICE} R	AACAGGCGTTCAAAGCGAAGC
Site-directed mutagenesis primers	**Sequence**
pCS2-Rab11b-GFP F - c.209A>T - Gln70Leu	CACCGCTGGCCTGGAGCGCTACC
pCS2-Rab11b-GFP R - c.209A>T - Gln70Leu	GGTAGCGCTCCAGGCCAGCGGTG
pCR-TBC1D8B full F - c.738G>C - Gln246His	TAATGGCATAGTTTGCCAGGTGTTCCATAAGAAGGTATG
pCR-TBC1D8B full R - c.738G>C - Gln246His	CATACCTTCTTATGGAACACCTGGCAAACTATGCCATTA
pCR-TBC1D8B full F - c.872T>C - Phe291Ser	CTTTGGGCAGCCTAGAAAAGGCATTAAATTGCTCACTGTGG
pCR-TBC1D8B full R - c.872T>C - Phe291Ser	CCACAGTGAGCAATTTAATGCCTTTTCTAGGCTGCCCAAAG
Primers for WISH probes	**Sequence**
Tbc1d8b F WISH1	GTTTGGTTTGCCGCAGAGAG
Tbc1d8b R WISH1	AATTAACCCTCACTAAAGGTCTCTGGAACTCCTCGCAC
Tbc1d8b F WISH2	ACGGGAATATCAGCTCTGCG
Tbc1d8b R WISH2	TAATACGACTCACTATAGGGAAGATGGAAGGCTGACCGTG
Tbc1d8b genotyping F	GCATCTTGCCATTGCTGATATTG
Tbc1d8b genotyping R	CAAGCCAACAGACATCTGTGAACC

Table S1 – List of primers used for experiments

Methods

ES and Mutation Calling

ES of DNA from families was performed using the Agilent SureSelect All Exon 51Mb V5 capture-kit and HiSeq2500 (Illumina) sequencer (paired-end reads: 2x75 bases). Obtained sequences were aligned to the human genome (National Center for Biotechnology build 37/hg19) using the Lifescope suite from Life Technologies. Substitution and variation calls were made with the Genome Analysis Toolkit pipeline. Variants were then annotated using the Paris Descartes University Bioinformatics platform software system. We assumed the causal variant (1) segregates with disease status; (2) is novel or has a minor allele frequency <1/1000 in dbSNP, 1000 Genome Project, gnomAD; (3) is not found in >10/2049 projects from our in-house database and (4) alters a protein's amino-acid sequence and is likely to disrupt the function of that protein according to PolyPhen2, SIFT, and MutationTaster.

Plasmids and cell culture

Human TBC1D8B ORF was obtained from Source BioScience (IRCMp5012H0832D) in a pCR-blunt II TOPO backbone (pCR-TBC1D8B-full). The Rab-Binding-Domain (aa1392 to 1412) of TBC1D8B was amplified using specific primers (Table S1) and then subcloned inframe into *BamHI* and *EcoRI* sites of plasmid pCS2-GFP (pCS2-RBD-GFP), into *KpnI* and *BamHI* sites of plasmids pmCherry-N1 (Clontech) (pN1-RBD-mcherry) and pCDNA3.1(+)/Myc-His C from Thermofischer (pCDNA-RBD-Myc). Zebrafish *tbc1d8b* 5'UTR and the 73 first bases of the cDNA were subcloned inframe into *BamHI* and *XhoI* sites of pCS2-GFP (PCS2-5'UTR-GFP) using primers listed in the table S1. Rab11b cDNA was amplified from a human podocyte cell line[1] using specific primers (Table S1) and then subcloned into *BamHI* and *EcoRI* sites of the pCS2-GFP plasmid (pCS2-Rab11b-GFP). All plasmids pDest-CA-rab5-GFP and pDest-CA-rab11a-GFP corresponding to the constitutively active form of each Rab were a kind gift from Dr. Stéphanie Miserey-Lenkei. Site-directed mutagenesis (QuikChange kit, Stratagene) was used to generate the missense mutations used in this study: p.Gln246His and p.Phe291Ser for TBC1D8B, and p.Gln70Leu for Rab11b to obtain the constitutively active form of Rab11b. All constructs were verified by Sanger sequencing.Human.

Embryonic Kidney 293T (HEK293T) cells were maintained in Dulbecco's Modified Eagle Medium (DMEM, Gibco®, Life Technologies) supplemented with 10% fetal bovine serum (FBS), glutamine and penicillin/streptomycin. Fibroblasts obtained from skin biopsies from affected and control individuals were cultured in OptiMEM (Gibco®, Life Technologies) supplemented with 10% FBS, glutamine, penicillin/streptomycin. Conditionally immortalized human podocytes (Saleem MA *et al.* 2002)[1] were

routinely cultured at 33°C in RPMI-1640 (Gibco®, Life Technologies), supplemented with 10% FBS, 1% insulin/transferrin/selenium, glutamine and penicillin/streptomycin (all from Life Technologies), and then, for experiments, cells were thermoswitched to 37°C for 10-14 days differentiation. Cells used in this study were tested mycoplasma-free.

Antibodies, reagents and chemical compounds

The following antibodies were used in this study: mouse monoclonal antibodies (mAb) against GFP [Roche, Cat. No. 118144600001, used at 1/2000 for western blot (WB)], c-myc epitope (Thermo Fisher, MS-139-P1, used at 1/1000 for WB), and synaptopodin [Progen, Cat. No. 65194, used at 1/40 for immunofluoresence (IF)], and rabbit polyclonal antibodies against TBC1D8B (Abcam, ab121780, used at 1/50 for IF and ab179995, used at 1/1000 for WB) and Rab11b (Atlas Antibodies HPA054396, used at 1/200 for IF). Alexa-fluor 647 Phalloidin from Thermofischer was used for IF (catA22287). For IF, Alexa Fluor-conjugated secondary antibodies (donkey anti-rabbit Alexa Fluor 488 and anti-mouse Alexa Fluor 546) were obtained from Life Technologies (ThermoFischer). Alexa-Fluor 555- or 546-conjugated transferrin (Life Technologies, Cat.No T35352 and T23364, respectively, used at 25µg/mL) was used for trafficking experiments.

Immunoprecipitation and immunoblotting

HEK293T cells were transiently co-transfected with pcDNA3.1-RBD-myc and either pDest-CA-Rab5/11a-GFP or pCS2-CA-Rab11b-GFP using Lipofectamine Reagent 2000 (ThermoFischer Scientific) according to the manufacturer instructions. Forty-eight hours post transfection, cells were lysed in 50 mM Tris-HCl pH8, 150 mM NaCl, 1% NP-40 supplemented with 10 mM protease inhibitor cocktail (Sigma) and incubated for 20 min at 4 °C. After centrifugation (10min, 10 000 rpm, 4°C), protein dosage was performed using the BCA protein assay kit (Thermo Scientific). The c-myc tag was immunoprecipitated using the µMACS™ Epitope Tag Protein Isolation Kit (Miltenyi Biotec). Briefly, fresh lysates (1mg of protein) were incubated with magnetic beads coupled to a myc antibody. For immunoprecipitation of endogenous TBC1D8B, HEK293T lysates were incubated with rabbit anti-TBC1D8B antibodies (1µg), followed by a 30-min incubation with magnetic beads-coupled to protein A. Immunoprecipitated proteins were isolated using µMACS™ Separation Columns in a magnetic µMACS™ separator and subsequently eluted with 1X Laemmli buffer. Lysates (50µg) and immunoprecipitated samples were loaded on a 8-16 % Mini-PROTEAN® TGX™ precast gel (BioRAD) and transferred to a PVDF membrane (GE Healthcare). Immunoblotting was performed using the indicated primary antibodies overnight at 4°C and the secondary antibodies for 1 hour at room temperature. Signals were detected using ECL reagents (Amersham Biosciences) and acquired with a Fusion Fx7 imaging system (Vilber Lourmat).

Immunofluorescence and vesicular trafficking studies

Podocytes were grown on type I collagen-coated coverslips and either used to study the subcellular localization of endogenous TBC1D8B, or transiently transfected the next day using FuGENE® HD Transfection Reagent (Promega) or used for endocytosis and recycling experiments. Cells were fixed in 4% paraformaldehyde (PFA) for 20 min at room temperature and alternatively permeabilized with 0.3% Triton TX-100 (Sigma) in 1X PBS for 4 min (for endogenous TBC1D8B) or directly incubated in blocking buffer containing 5% bovine serum albumin (BSA, Sigma) for 1h at room temperature. Cells were then incubated in the appropriate primary and secondary antibodies for 1h each at room temperature. Nuclei were stained with Hoechst (#33342, Sigma) at room temperature for 8 min.

For transferrin endocytosis (uptake) / recycling (chase), we performed two different analyses:

For endocytosis study (transferrin uptake), fibroblasts were starved at 37°C for 60 min in transferrin-free OptiMEM medium supplemented with 1% Bovine Serum Albumin (BSA) and podocytes were starved in Serum-Free-Medium devoid of transferrin (SFM, Gibco®, Life Technologies) with 1% Bovine Serum Albumin (BSA) for 60 min. Cells were then incubated on ice at 4°C in the same ice-cold medium enriched with Alexa-Fluor (AF-555)-conjugated transferrin at a final concentration of 25µg/mL. This step allows transferrin to bind its receptor but inhibit internalization. After 30 min incubation, cells were washed in cold 1X PBS. Cells were then incubated at 37°C in their respective medium (with transferrin) to allow transferrin internalization, and blocked in 4% PFA at different time points. Mutated cells were compared to control cells for each time point.

For recycling study (chase study), cells were incubated in Alexa-conjugated transferring-enriched appropriate medium (25µg/mL) supplemented with 1% BSA for 60min at room temperature for fibroblasts and 120min for podocytes. Cells were then washed with 1X PBS, incubated in transferrin-free medium and then fixed in 4% PFA at different time points. For endocytosis and recycling, all time points' results were normalized to T0.

As transferrin endocytosis / recycling kinetics are dependent on cell types, the use of different time points for transferrin endocytosis and chase in podocytes vs fibroblasts were based on the manufacturer instructions (30 to 60 min for endocytosis) and literature when available[1,2,3], and empirically on our personal lab experience. Experiments were repeated 3 times and at least 20 cells were analyzed in each time point experiment. Microscope settings were the same within each independent experiment. The integrated fluorescence intensity in each independent cell was measured and the background fluorescence intensity was subtracted to calculate corrected total cell

fluorescence (CTCF) using the following equation CTCF=integrated density − (area of selected cell × mean background fluorescence per unit area). All time point values were normalized to T0 (maximum intensity). Whereas microscope settings allow to easily detecting a 50% decrease of fluorescence in cells, they were imprecise for lower values. Thus recycling assay was stopped when the fluorescence intensity in WT cells reached 50% of the intensity measured at T0.

Immunofluorescence studies of endogenous TBC1D8B were performed as described above on 10 µm-frozen sections of human embryonic kidney biopsies obtained from The Department of Pathology of Necker-Enfants Malades Hospital (Paris, France).

Scratch assay and adhesion assay

This was performed as previously described by Vollenbroker *et al.,* 2009[2]. In brief, confluent differentiated human podocytes were cultured in six-well plates and scratched with two lines at 90° angle with a sterile 0.4-mm 200-µl Gilson style extension length tip. Images of the same field were captured at 0 and 12 hours.

Medium was removed, and cells were trypsinized until all cells were suspended, which was optically controlled. Cells were plated into 96-well plates and three experimental wells were assigned as the 100% attachment control, to which 20%, 50% and 100% of the total volume of cells were added. Cells were left to adhere for 45 min at 37^{o}C. Control wells for 100% attachment were fixed with 100 µl 4% PFA for 20 min at room temperature. Thereafter, the plate was tapped to remove lose and non-adherent podocytes, and washed twice with 100 µl PBS, and the experimental wells were then fixed with 100 µl 4% PFA for 20 min. Cells were stained with 100µl of 0.1% crystal violet in 2% ethanol for 60 minutes at room temperature. Absorbance on the plate was measured at 570nM in a plate reader. Results were depicted as a percentage of 100% adherent cells and normalized against the adhesion of the human wild type podocytes.

Zebrafish

Breeding and embryo collection

Adult zebrafish were maintained in system water at 28 °C, pH 7 and conductivity of 500µS on a 14 h light/10 h dark cycle. They were bred by natural crosses and embryos were maintained at 28 °C in embryo medium (0.1 g/L Instant Ocean Sea Salts, 0.1 g/L sodium bicarbonate, 0.19 g/L calcium sulphate, 0.2 mg/L methylene blue, H_2O) until the desired developmental stage was reached.

Morpholinos

To knockdown the expression of *tbc1d8b*, *tbc1d8b* splice-blocking morpholino (MO^{SPLICE}-GAGCAAAATAACCATCTCACCCTTA) targeting the exon3-intron3 boundary, and translation-blocking morpholino (MO^{ATG}-TTGAGCCACATGCTGGAATTTGTCT) targeting the ATG codon were designed and ordered from GeneTools, LCC. The following mismatch control morpholino ($MO^{CONTROL}$-CTAGGACGGACACGTGTTACCCAGG) was used as a negative control. Dose-response experiments were performed to determine the optimum concentration of morpholino which produced no toxic effects. A 8 ng/embryo dose of the *tbc1d8b* splice morpholino yielded a reproducible phenotype, whereas injection of the control did not result in any detectable phenotype at the same dose. A dose of 1.6 ng/embryo was determined for the *tbc1d8b* translation-blocking morpholino. The morpholinos were injected into embryos at the 1–2 cell stage with phenol red as a vehicle to visualise injections. After microinjection, embryos were maintained as described above. Embryo development was evaluated at 24 hpf, 48 hpf, 72 hpf and 96hpf.

Splice morpholino specificity was checked by RT-PCR. Briefly, mRNA was isolated using Qiagen Extraction Kit and then treated with DNase I. Five micrograms of total RNA was reverse-transcribed using Superscript II (Life Technologies) with oligo(dT) primers. PCR was the performed using the primers listed in Table S1.

For translation-blocking morpholino specificity check, mRNA was synthesized from pCS2-5'UTR-GFP using the SP6 mMessage mMachine Kit from Thermo Fisher. Briefly, 5 µg of plasmid were linearized (*NotI*) and purified in 15µL H2O. 6 µL were used to synthesize mRNA. After synthesis, mRNA yield was measured using a nanodrop technology. MO^{ATG} specificity was checked by co-injection of the newly synthesized mRNA with the MO^{ATG}. The absence of GFP confirmed the efficacy of MO^{ATG}.

Whole-mount *in situ* hybridization (WISH)

WISH probes were synthesized using specific primers listed in the table S1. T3 enzyme was used for *tbc1d8b* transcription and digoxigenin labeling. For whole-mount *in situ* hybridization, embryos were fixed in PFA 4% overnight at 4 °C and processed as described in Thisse and Thisse, 2008{Thisse, 2008 #506}.

Proteinuria analyses

For proteinuria screening, embryos were injected at 96hpf directly in the cardinal vein with both a FITC-labeled 500kDa and Texas-Red-labeled 10kDa dextrans (20mg/mL each - 4nL).

For the eye dye filtration assay, fluorescence was measured in retinal vein at 1hpi and 24hpi. Normalized CTCF were calculated as described previously and compared for each condition.

For tubular assay, fish were fixed 6hours after dextran injection in 4% PFA and embedded in technovit® 7100 from EMS (#14653) according to the manufacturer protocol.

Rescue experiments

mRNA was synthesized from pCR-TBC1D8B-full WT and mutated after *BamHI* restriction using the T7 promoter. Briefly, 1µg of linearized plasmid was used form mRNA synthesis using the mMessage mMachine Kit from ThermoFischer. Each newly synthesized mRNA was then titrated and co-injected with MO^{ATG} and MO^{SPLICE} in the cytoplasm of 1 cell-stage embryos and phenotype was screened at day 4.

Transmission electron microscopy and Imaging

For transmission electron microscopy, human samples were washed three times in 0.1 M cacodylate buffer at 4°C and postfixed in 1% osmium tetroxide in 0.1 M cacodylate buffer before dehydration with ethanol. This was followed by embedding them in Araldite resin. Zebrafish embryo were fixed in 4% PFA and 4% glutaraldehyde in PBS overnight at 4°C, and then dehydrated through a graded ethanol series. Samples were embedded in epoxy resin (Electron Microscopy Sciences). For all samples ultra-thin sections (50-90 nm) were obtained using a Reichert Ultracut S (Leica, Germany), and these were placed on 75-mesh grids (Electron Microscopy Sciences) and conventionally stained with uranyl acetate and lead citrate (Electron Microscopy Sciences). Observations and images were collected using a JEOL 1011 transmission electron microscope operating at 80 kV and equipped with a GATAN Orius camera 1000 for zebrafish and digital micrographs were taken on a Philips 100CS microscope for human samples.

Depending on the experiments performed on human or zebrafish tissue, samples were examined with different microscopes: a Leica M165FC stereoscope, an epi-illumination microscope (DMI 6000, Leica) with a cooled charge-coupled device (CCD) camera (MicroMax, Princeton Instruments), a spinning disc confocal composed by a Yokogawa CSU-X1 spinning disk scanner coupled to a Zeiss Observer Z1 inverted microscope through a Hamamatsu Orca Flash 4.0 sCMOS Camera, and a Leica SP5-II confocal laser scanning microscope attached to a Leica DMI 6000 inverted epifluorescence microscope.

Statistical analysis

Statistical analysis of at least three independent experiments was done using the one-sample two tailed *t* test and proportions were compared using the Chi2 test. *p* values: *, $p<0.05$; **, $p<0.01$; ***, $p<0.001$. GraphPad Prism 5 software was used to perform all statistical analyses (mean± SEM).

Additional references

1. Saleem, M.A., O'Hare, M.J., Reiser, J., Coward, R.J., Inward, C.D., Farren, T., Xing, C.Y., Ni, L., Mathieson, P.W., and Mundel, P. (2002). A conditionally immortalized human podocyte cell line demonstrating nephrin and podocin expression. J Am Soc Nephrol 13, 630-638.
2. Vollenbroker, B., George, B., Wolfgart, M., Saleem, M.A., Pavenstadt, H., and Weide, T. (2009). mTOR regulates expression of slit diaphragm proteins and cytoskeleton structure in podocytes. Am J Physiol Renal Physiol 296, F418-426.
3. Rapaport D, Lugassy Y, Sprecher E, Horowitz M. Loss of SNAP29 impairs endocytic recycling and cell motility. *PLoS One.* 2010;5(3):e9759.
4. Romano S, Maffei P, Bettini V, et al. Alstrom syndrome is associated with short stature and reduced GH reserve. *Clin Endocrinol (Oxf).* 2013;79(4):529-536.
5. Hermle T, Schneider R, Schapiro D, et al. GAPVD1 and ANKFY1 Mutations Implicate RAB5 Regulation in Nephrotic Syndrome. *J Am Soc Nephrol.* 2018;29(8):2123-2138.